ELSEVIER

J. Non-Newtonian Fluid Mech. 143 (2007) 120–130

Journal of Non-Newtonian Fluid Mechanics

www.elsevier.com/locate/jnnfm

Electrohydrodynamic instability of a confined viscoelastic liquid film

Gaurav Tomar [a], V. Shankar [b,*], Ashutosh Sharma [b,**], Gautam Biswas [a]

[a] *Department of Mechanical Engineering, Indian Institute of Technology, Kanpur 208016, India*
[b] *Department of Chemical Engineering, Indian Institute of Technology, Kanpur 208016, India*

Received 5 September 2006; received in revised form 25 December 2006; accepted 8 February 2007

Abstract

We study the surface instability of a confined viscoelastic liquid film under the influence of an applied electric field using the Maxwell and Jeffreys models for the liquid. It was shown recently for a Maxwell fluid in the absence of inertia that the growth rate of the electrohydrodynamic instability diverges above a critical value of Deborah number [L. Wu, S.Y. Chou, Electrohydrodynamic instability of a thin film of viscoelastic polymer underneath a lithographically manufactured mask, J. Non-Newtonian Fluid Mech. 125 (2005) 91] and the problem of pattern length selection becomes ill-defined. We show here that inclusion of fluid inertia removes the singularity and leads to finite but large growth rates for all values of Deborah number. The dominant wavelength of instability is thus identified. Our results show that the limit of small inertia is not the same as the limit of zero inertia for the correct description of the dynamics and wavelength of instability in a polymer melt. In the absence of inertia, we show that the presence of a very small amount of solvent viscosity (in the Jeffreys model) also removes the non-physical singularity in the growth rate for arbitrary Deborah numbers. Our linear stability analysis offers a plausible explanation for the highly regular length scales of the electric field induced patterns obtained in experiments for polymer melts. Further, the dominant length scale of the instability is found to be independent of bulk rheological properties such as the relaxation time and solvent viscosity.

Keywords: Electrohydrodynamic instability; Viscoelastic instability; Thin films

1. Introduction

Lithography-induced self assembly ("LISA") has emerged as a simple and useful technique to produce small-sized periodic features [1,2], which utilizes an electric field induced surface roughening of a polymer film. An electric field is applied across a lithographically produced mask and a substrate with a polymeric liquid (i.e. a polymer above its glass transition temperature) on it. Due to the applied/induced electric field, the polymer film (which could be a leaky or perfect dielectric) gets polarized with free and bound charges appearing on its surface. The electrostatic force on these charges disrupts the stability of the initially flat film surface, thereby causing its roughening (Fig. 1). The wavelength of the resultant patterns is selected by a competition between the destabilizing electrostatic forces and stabilizing surface tension force. The LISA technique may find applications in patterning of electrical, optical and bio-engineering devices [1–6]. The electric field induced instability, modulated further by the use of a patterned electrode [3], can thus be employed for engineering of desired periodic lattices in thin polymer films. There is thus considerable interest in the theoretical understanding of the underlying phenomenon, which will also help in devising new strategies for self-organized patterning.

The surface instability of a Newtonian fluid (modeled as both leaky and perfect dielectrics) under the effect of electric field is now well understood [4,7–9]. Pease and Russel [4] established that the wavelength of the fastest-growing mode for leaky dielectrics decreases substantially compared to the perfect dielectric case. Even a small amount of conductivity can cause a substantial change in the wavelength (decreases by 2–4 times) and the growth rate (increases by 2–20 times) for the same applied potential. Surface instability of a soft solid elastic film subjected to an external electric field has also been studied, both experimentally and theoretically [10,11]. It was observed that the wavelength of the patterns in purely elastic films remains unaltered with change in the strength of electric field and depends only on thickness of the confined film. In another recent study, Wu and Chou [12] performed linear stability analysis of a

* Corresponding author. Tel.: +91 512 259 7377; fax: +91 512 259 1014.
** Corresponding author.
E-mail addresses: vshankar@iitk.ac.in (V. Shankar), ashutos@iitk.ac.in (A. Sharma).

0377-0257/$ – see front matter © 2007 Elsevier B.V. All rights reserved.
doi:10.1016/j.jnnfm.2007.02.003

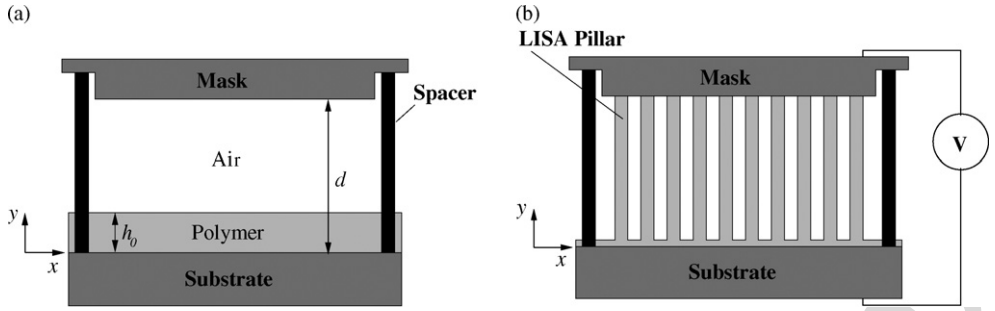

Fig. 1. (a) Schematic representation of the configuration of the polymer prior to the application of an electric field. (b) Schematic representation of the LISA pillar formation on application of an electric field.

leaky-dielectric viscoelastic fluid whose constitutive behavior was described using the Jeffreys model [13,14]. Their analysis assumed the creeping-flow approximation (i.e. zero inertia limit) to be valid in the entire range of Deborah numbers. The Deborah number, *De*, is the non-dimensional relaxation time characterizing the extent of elasticity in the viscoelastic liquid. Wu and Chou [12] showed that the wavelength corresponding to the maximum growth rate remains unchanged with *De*, below a certain critical *De*. Interestingly, they obtained unbounded growth rate in case of a polymer melt (i.e. for a Maxwell fluid where there is no solvent contribution to the stress) at a critical Deborah number. Above this critical Deborah number, the growth rate diverged at two wavenumbers between which a window of stable wavenumbers was also observed. The wavenumbers at which this divergence occurs were found to depend on the Deborah number. The dominant instability mode corresponds to the maximum growth rate, which, however, cannot be determined in the inertia-less analysis as shown in this paper. The divergence of growth rate and the non-physical behavior of the film between the two critical wavenumbers thus preclude the determination of the dominant wavelength of the instability and the resulting pattern pitch.

In a recent study [15] of dewetting of a thin viscoelastic polymer melt due to van der Waals force, we observed a profound influence of inertia in regularizing the dispersion relation for ultra thin films. It was also found that for polymer solutions, even a small amount of solvent viscosity removed the divergence by providing an additional mode of energy dissipation, even in the absence of inertia. Similar conclusions were reached in the earlier study by Aitken and Wilson [16] for the Rayleigh-Taylor instability of a viscoelastic liquid film. In this paper, we revisit the linear stability analysis of a viscoelastic liquid film confined between two electrodes. We show that the unbounded growth rates obtained for the thin films of polymer melt under the creeping-flow approximation [12] are non-physical in that inclusion of inertia removes the singularity, which makes it possible to predict the lengthscale of the instability. We thus show that inertial effects, which are considered negligible in a polymeric thin film, cannot be completely neglected in the description of dynamics of the instability. Even in the absence of inertia, with a very small amount of solvent (modeled by the Jeffreys model), the growth rates obtained for large Deborah numbers are finite. In what follows, we formulate the problem in Section 2. Linear stability analyses of the system with and without inclusion of inertial terms and solvent viscosity are presented in Section 3. Representative results are presented and discussed in Section 4. We summarize the salient conclusions of this study in Section 5.

2. Formulation

We consider a polymer film of thickness h_0 confined between two flat electrodes separated by a distance d (Fig 1(a)). On application of an electric field between the electrodes, a negative pressure is generated in the film which makes the film surface deform and leads to the formation of pillar-like structures (Fig. 1(b)).

2.1. Governing equations and boundary conditions

The polymeric liquid is considered to be incompressible and thus the continuity equation reduces to:

$$\nabla \cdot \mathbf{u} = 0, \tag{1}$$

where $\mathbf{u} = (u, v)$ is the velocity field in the polymeric liquid. The momentum balance for the polymeric liquid is given by

$$\rho \frac{D\mathbf{u}}{Dt} = -\nabla p + \nabla \cdot \boldsymbol{\tau}, \tag{2}$$

where D/Dt is the substantial derivative, $\boldsymbol{\tau}$ the extra-stress tensor (discussed below) and p is the isotropic pressure.

The viscoelastic nature of the polymeric liquid may be adequately captured by using an Oldroyd-B model, which incorporates fading memory in a polymer solution, as well as predicts first normal-stress differences. However, we examine here the stability of a quiescent, static base state under the influence of electric fields. Any non-linearities that appear due to the upper convected terms in the Oldroyd-B model (which render the model material-frame indifferent) will not make any contributions in the linearized analysis about the static base state. Hence, without loss of generality, we can examine the stability of the viscoelastic fluid described by a general linear viscoelastic model, which is described by the constitutive relation

$$\boldsymbol{\tau}(t) = \int_{-\infty}^{t} G(t - t')\mathbf{D}(t')\,\mathrm{d}t', \tag{3}$$

where $G(t - t')$ is the stress-relaxation modulus describing the viscoelastic behavior of the material and $\mathbf{D} = 1/2(\nabla\mathbf{u} + \nabla\mathbf{u}^T)$

is the rate-of-deformation tensor. When the upper-convected time derivative is replaced by a partial time derivative, the Oldroyd-B model reduces to a Jeffreys model. The relaxation modulus for the Jeffreys model is given by [14]:

$$G(t-t') = \frac{\eta_0}{\lambda_1}\left[\left(1-\frac{\lambda_2}{\lambda_1}\right)\mathrm{e}^{-(t-t')/\lambda_1} + 2\lambda_2\delta(t-t')\right], \quad (4)$$

where $\delta(t-t')$ is the Dirac delta function, λ_1 the relaxation time and λ_2 is the retardation time. The total viscosity of the polymeric liquid $\eta_0 = \eta_p + \eta_s$ is the sum of polymer viscosity (η_p) and solvent viscosity (η_s). The relation between the relaxation time and retardation time is given by:

$$\lambda_2 = \lambda_1\frac{\eta_s}{\eta_0}. \quad (5)$$

Defining $\delta = \eta_s/\eta_0$ as the ratio of solvent to total viscosities, we observe that if $\delta = 0$ we obtain the case of pure polymer melt (Maxwell fluid). For the case $\delta = 1$ or $\lambda_1 = \lambda_2$, the Jeffreys model reduces to simple Newtonian fluid.

The Maxwell laws of electrodynamics in conjunction with hydrodynamics have been modeled using the Taylor-Melcher leaky dielectric model [17,18]. Neglecting the magnetic induction due to charge movement (low dynamics current), the Maxwell laws essentially reduce to electrostatics. The Maxwell equations governing the electric fields in the polymer (subscript I) and air (subscript II) are given by:

$$\nabla\cdot\mathbf{E}_I = 0, \quad (6)$$

$$\nabla\times\mathbf{E}_I = 0, \quad (7)$$

$$\nabla\cdot\mathbf{E}_{II} = 0, \text{ and} \quad (8)$$

$$\nabla\times\mathbf{E}_{II} = 0. \quad (9)$$

The parameter ϵ is the relative permittivity of the viscoelastic film and ϵ_0 is the permittivity of the vacuum. The electric field, by virtue of its curl being zero everywhere in the medium, can be written using a potential function as $\mathbf{E} = -\nabla\phi$. Therefore, governing equations for the electric field in region-I and -II can now be written as:

$$\nabla^2\phi_I = 0, \text{ and} \quad (10)$$

$$\nabla^2\phi_{II} = 0, \text{ respectively.} \quad (11)$$

The Maxwell stress tensor describing the stress field induced in the material due to electrostatic forces in a leaky dielectric material is given by:

$$\mathbf{M} = \epsilon\epsilon_0\left(\mathbf{EE} - \frac{1}{2}(\mathbf{E}\cdot\mathbf{E})\mathbf{I}\right). \quad (12)$$

Boundary conditions for the above set of electrohydrodynamic governing equations are given below.

No slip boundary condition at the bottom surface:

$$u(0) = 0,\ v(0) = 0. \quad (13)$$

The top surface of the film is a free surface; therefore, the stress boundary condition is that of zero tangential stress:

$$\mathbf{n}\cdot(\|-p\mathbf{I}+\boldsymbol{\tau}\|)\cdot\mathbf{t} + q\mathbf{E}\cdot\mathbf{t} = 0, \quad (14)$$

where q is the free charge at the free surface which is governed by:

$$\frac{\partial q}{\partial t} + \mathbf{u}\cdot\nabla_s q = q(\mathbf{n}\cdot(\mathbf{n}\cdot\nabla)\mathbf{u}) + \|-\sigma\mathbf{E}\cdot\mathbf{n}\|. \quad (15)$$

Here, ∇_s is the surface gradient at the free surface of the film and σ is electrical conductivity of the fluid. The notation $\|.\|$ denotes the jump across the interface from region-I (polymer) to region-II (air).

Kinematic condition at the free surface of the film:

$$v(h) = \frac{\partial h}{\partial t} + u_s\frac{\partial h}{\partial x}. \quad (16)$$

Normal stress balance at the free surface yields:

$$(\|-p\mathbf{I}+\boldsymbol{\tau}\|\cdot\mathbf{n})\cdot\mathbf{n} + \frac{1}{2}\|\epsilon\epsilon_0(\mathbf{E}\cdot\mathbf{n})^2 - \epsilon\epsilon_0(\mathbf{E}\cdot\mathbf{t})^2\| + \frac{\gamma h_{xx}}{(1+h_x^2)^{3/2}} = 0, \quad (17)$$

where γ is the surface tension of the liquid–gas interface.

The contact electric potentials which could be present due to discontinuity of the medium across the interface are neglected and boundary conditions are applied assuming the effect of external applied potential alone, which is considered to be dominant. Electric potential at the bottom surface is set to be zero:

$$\phi_I = 0 \text{ at } y = 0. \quad (18)$$

Across the free surface, the electric potential is continuous:

$$\phi_{II} = \phi_I \text{ at } y = h. \quad (19)$$

A constant electric potential is set at $y = d$:

$$\phi_{II} = \phi_0 \text{ at } y = d. \quad (20)$$

The jump condition in the electric displacement across the free surface is equal to the free charge conducted through the leaky dielectric to the free surface and is given by the equation below:

$$\|\epsilon\epsilon_0\mathbf{E}\|\cdot\mathbf{n} = \|\epsilon\epsilon_0\frac{\partial\phi}{\partial\mathbf{n}}\| = q \text{ at } y = h. \quad (21)$$

3. Stability analysis

The system described by the governing equations and boundary conditions in the previous section is subjected to small two-dimensional perturbations to obtain its linear stability characteristics. The homogeneous or base state solutions of the governing equations are first solved and the solutions thus obtained are perturbed to give the dispersion relation between the wavenumber and the associated growth rate.

3.1. Base state solutions

The base state solutions are obtained by assuming a quiescent initial state; therefore, the base state velocity and viscoelastic

stresses in the film are zero. A general solution of the electric field equations (Eqs. (10) and (11)) yields:

$$\bar{\phi}_{\mathrm{I}} = A_1 y + B_1, \text{ and} \tag{22}$$

$$\bar{\phi}_{\mathrm{II}} = A_2 y + B_2. \tag{23}$$

Eq. (15) in absence of any motion of the interface reduces to:

$$\frac{\partial q}{\partial t} = \sigma \mathbf{E}_{\mathrm{I}} \cdot \mathbf{n}. \tag{24}$$

The steady state solution of the above equation implies that $\mathbf{E}_{\mathrm{I}} \cdot \mathbf{n} = 0$ if the conductivity is not zero, that is even a slightest of conductivity can lead to zero electric field in the film. However, if the conductivity is absolutely zero the electric field obtained is that corresponding to the perfectly dielectric case. Using the solution given by Eqs. (22) and (23) and substituting zero electric field condition, we get $A_1 = 0$. Applying zero-potential boundary condition (Eq. (18)), we get $B_1 = 0$. Therefore, the base state electric potential in region-I is $\bar{\phi}_{\mathrm{I}} = 0$. Using Eqs. (19) and (20), we obtain the base state electric potential in region-II as given below:

$$\bar{\phi}_{\mathrm{II}} = \frac{\phi_0 (y - h_0)}{(d - h_0)}. \tag{25}$$

Now, using the equation for jump in the electric displacement vector (Eq. (21)), we get the base state free-charge at the free surface of the film:

$$\bar{q} = \frac{\phi_0 \epsilon_0}{d - h_0}. \tag{26}$$

The normal stress balance equation at the free surface of the film yields the base state pressure field:

$$\bar{p} = -\frac{1}{2}\epsilon_0 \left(\frac{\phi_0}{(d - h_0)} \right)^2. \tag{27}$$

3.2. Linearized governing equations and boundary conditions

In order to perform linear stability analysis, we linearize the governing differential equations and the boundary conditions about the above-defined base state. Small fluctuations in the form of Fourier modes are imposed on the base-state variables as given below, where k is the wavenumber of the perturbations and s is the growth rate:

$$h = h_0 + \tilde{h} \mathrm{e}^{ikx} \mathrm{e}^{\mathrm{st}}, \tag{28}$$

$$q = \bar{q} + \tilde{q} \mathrm{e}^{ikx} \mathrm{e}^{\mathrm{st}}, \tag{29}$$

$$u = \tilde{u}(y) \mathrm{e}^{ikx} \mathrm{e}^{\mathrm{st}}, \tag{30}$$

$$v = \tilde{v}(y) \mathrm{e}^{ikx} \mathrm{e}^{\mathrm{st}}, \tag{31}$$

$$p = \bar{p} + \tilde{p}(y) \mathrm{e}^{ikx} \mathrm{e}^{\mathrm{st}}, \tag{32}$$

$$\boldsymbol{\tau} = \tilde{\boldsymbol{\tau}} \mathrm{e}^{ikx} \mathrm{e}^{\mathrm{st}}, \tag{33}$$

$$\phi_{\mathrm{I}} = \tilde{\phi}_{\mathrm{I}}(y) \mathrm{e}^{ikx} \mathrm{e}^{\mathrm{st}}, \tag{34}$$

$$\phi_{\mathrm{II}} = \bar{\phi}_{\mathrm{II}}(y) + \tilde{\phi}_{\mathrm{II}}(y) \mathrm{e}^{ikx} \mathrm{e}^{\mathrm{st}}. \tag{35}$$

Using the constitutive relation (Eq. (3)) with the relaxation modulus $G(t)$ for the Jeffreys viscoelastic fluid (Eq. (4)), we obtain:

$$\tilde{\boldsymbol{\tau}}(y) = \eta(s) \tilde{\mathbf{D}}(y), \tag{36}$$

where $\tilde{\mathbf{D}}(y) = 1/2(\nabla \tilde{\mathbf{u}} + \nabla \tilde{\mathbf{u}}^T)$ and $\eta(s) = \eta_0(1 + \lambda_2 s)/(1 + \lambda_1 s)$ is the Laplace transform of the stress relaxation modulus. For $\lambda_1 = \lambda_2$, Eq. (36) reduces to that for a Newtonian fluid, for $\lambda_2 = 0$, the constitutive relation is that for a Maxwell fluid. Thus, in this linearized stability analysis about the static base state, the only way in which viscoelasticity appears in the calculation is through the growth-rate dependence of viscosity. In principle, one could therefore obtain the dispersion relation relating the growth rate to the wavenumber by simply substituting the the frequency-dependent viscosity $\eta(s)$ instead of the constant viscosity in the characteristic equation for a Newtonian fluid. However, such a result is available only in the long-wave limit for Newtonian liquid. Here, we would like to examine the dispersion relation for arbitrary wavenumbers, and hence it is necessary to carry out the stability calculation completely.

Linearizing the momentum equations in terms of the above perturbed variables, we obtain:

x-momentum equation:

$$-\tilde{p}(y)(ik) + \eta(s)[-k^2 \tilde{u}(y) + \tilde{u}''(y)] - \rho s \tilde{u}(y) = 0, \tag{37}$$

y-momentum equation:

$$-\tilde{p}'(y) + \eta(s)[2\tilde{v}''(y) - k^2 \tilde{v}(y) + (ik)\tilde{u}(y)] - \rho s \tilde{v}(y) = 0. \tag{38}$$

Simplifying the above two equations (Eqs. (37) and (38)) using linearized continuity equation ($\tilde{u}(y) = i/k \tilde{v}'(y)$) and eliminating the pressure term, we obtain a biharmonic equation (with respect to y) in the vertical component of the velocity:

$$\tilde{v}^{\mathrm{IV}} - (m^2 + k^2)\tilde{v}^{\mathrm{II}} + k^2 m^2 \tilde{v} = 0, \tag{39}$$

where $m^2 = k^2 + \rho s/\eta(s)$.

Linearized governing equations for electric potential in region-I (polymer fluid) and region-II (air) are:

$$-k^2 \tilde{\phi}_{\mathrm{I}} + \tilde{\phi}_{\mathrm{I}}'' = 0, \tag{40}$$

and

$$-k^2 \tilde{\phi}_{\mathrm{II}} + \tilde{\phi}_{\mathrm{II}}'' = 0. \tag{41}$$

A set of general solutions of the above ODE equations is given by:

$$\tilde{v}(y) = A \mathrm{e}^{ky} + B \frac{\mathrm{e}^{my} - \mathrm{e}^{ky}}{m - k} + C \mathrm{e}^{-ky} + D \frac{\mathrm{e}^{-ky} - \mathrm{e}^{-my}}{m - k}, \tag{42}$$

$$\tilde{\phi}_{\mathrm{I}}(y) = A_{\mathrm{I}} \mathrm{e}^{ky} + B_{\mathrm{I}} \mathrm{e}^{-ky}, \text{ and} \tag{43}$$

$$\tilde{\phi}_{\mathrm{II}}(y) = A_{\mathrm{II}} \mathrm{e}^{ky} + B_{\mathrm{II}} \mathrm{e}^{-ky}. \tag{44}$$

The constants A, B, C, D, A_{I}, B_{I}, A_{II} and B_{II} can be evaluated using the linearized boundary conditions (Eqs. (13)– (21)) given below.

No-slip boundary condition at the bottom surface of the thin film:

$$\tilde{v} = 0 \text{ at } y = 0, \tag{45}$$

$$\tilde{v}' = 0 \text{ at } y = 0. \tag{46}$$

Linearized kinematic boundary condition at $y = h$:

$$\tilde{v} = \tilde{h}s \text{ at } y = h. \tag{47}$$

Linearized zero shear stress boundary condition at $y = h$:

$$-\eta(s)(\tilde{v}'' + k^2\tilde{v}) + k^2\bar{q}\tilde{\phi}_{\mathrm{I}} = 0. \tag{48}$$

Potential at the bottom ($y = 0$) and the top electrodes ($y = d$) are maintained constant, therefore,

$$\tilde{\phi}_{\mathrm{I}}(0) = 0, \tag{49}$$

and

$$\tilde{\phi}_{\mathrm{II}}(d) = 0. \tag{50}$$

Continuity of the electric potential across the interface yields:

$$\tilde{\phi}_{\mathrm{I}}(h) = \tilde{\phi}_{\mathrm{II}}(h) + \frac{\phi_0\tilde{h}}{d - h_0}. \tag{51}$$

Linearized form of the jump across the interface in the electric displacement is given by:

$$\epsilon_0\tilde{\phi}'_{\mathrm{II}} - \epsilon\epsilon_0\tilde{\phi}'_{\mathrm{I}} = \tilde{q}. \tag{52}$$

Linearizing free charge conservation equation at the free surface yields:

$$\tilde{q}s = \bar{q}\tilde{v}'(h) - \sigma\tilde{\phi}'_{\mathrm{I}}(h). \tag{53}$$

Linearized normal stress balance equation at the free surface yields:

$$\tilde{p}(h) - 2\eta(s)\tilde{v}'(h) = -\epsilon_0\left(\frac{\phi_0}{d - h_0}\right)\tilde{\phi}'_{\mathrm{II}}(h) + \gamma\tilde{h}k^2. \tag{54}$$

The dispersion relation is obtained by solving for the coefficients using the above boundary conditions (Eqs. (46)–(53)) and substituting the solution in the linearized normal stress balance equation at the free surface (Eq. (54)). The dispersion relation so obtained can also be written in terms of the following non-dimensional groups defined as:

$$H_0 = \frac{h_0}{d}, \tag{55}$$

$$\bar{\gamma} = \frac{\gamma}{(\epsilon_0\psi_0^2/2h_0)}, \tag{56}$$

$$\bar{\sigma} = \frac{\bar{\gamma}}{4H_0^3}\frac{\sigma}{(\epsilon_0\psi_0^2/2\eta_0h_0^2)}, \tag{57}$$

$$De = \frac{4H_0^3}{\bar{\gamma}}\frac{\lambda\epsilon_0\psi_0^2}{2\eta_0h_0^2}. \tag{58}$$

The wavenumber is non-dimensionalized using the long length scale $L = h_0(\bar{\gamma}/(2H_0^3))^{1/2}$ and is represented by $K = kL$. Growth rate is non-dimensionalized using the long time scale $T = 2\bar{\gamma}\eta_0h_0^2/(4H_0^3\epsilon_0\psi_0^2)$, and the non-dimensional growth rate is given by $\bar{s} = sT$. In the following section, all the results and discussions are presented in terms of these non-dimensional parameters which are also in conformity with the ones used in Wu and Chou [12]. To simplify notation, we drop the bar in the non-dimensional growth rate $\bar{s}$ and from now on, use s to denote the non-dimensional growth rate.

A non-dimensional number R representing the strength of the inertial terms emerges from the analysis: $R = \rho\epsilon_0\phi_0^2/(2\eta_0^2)$. For typical values of the parameters, $\rho = 10^3$ kg/m^3, $\epsilon_0 = 8.85 \times 10^{-12}$ C^2 N^{-1} m^{-2}, $\eta = 1$ kg/m s and $\phi_0 = 100$ V, the value of the parameter R is 6×10^{-5}. The strength of the inertial terms as represented by R is indeed small and because R multiplies the growth rate in the governing momentum equations, it seems reasonable to neglect inertial terms in the analysis. However, as is shown below, when such an analysis predicts unbounded growth rates, the inertial terms can no longer be neglected because the product of R and the large growth rate is no longer negligible.

4. Results and discussion

The general full dispersion relation is given in Appendix A in the form of matrix elements, whose determinant is set to zero to obtain the dispersion relation.

4.1. Behavior of a thin Maxwell liquid film in the absence of inertia ($R = 0$, $\delta = 0$, $De \neq 0$)

The dispersion relation given in Appendix A reduces to the dispersion relation under the creeping-flow approximation in the limit of $R \to 0$. Under the long-wave assumption ($\bar{\gamma} \to \infty$), we have verified that our dispersion relation reduces to the dispersion relation derived in ref. [12]. We first present here results obtained using the full dispersion relation (i.e without the long-wave assumption) in order to demonstrate that the singularity of the growth rate obtained in Wu and Chou [12] is present even in the full dispersion relation and is thus not attributable to the terms neglected in the long-wave assumption.

Fig. 2 shows the variation of growth rate with non-dimensional wavenumber K for different values of De. The values of other parameters are $\bar{\sigma} = 1000$, $\bar{\gamma} = 500$, $\epsilon_1 = 2$ and $H_0 = 0.5$. The critical and the most dangerous wavelength is a function of $\bar{\gamma}$, H_0 and $\bar{\sigma}$ only and is independent of δ and De. For $De = 0$ (Newtonian fluid), the maximum growth rate is $s_{\max} = 0.665$ at wavenumber $K_{\mathrm{m}} = 1.97$. With increase in the Deborah number, the response time to any excitation decreases as the elastic behavior increases in the fluid. This decrease in the response time leads to an increase in the maximum growth rate with increase in De. However, the most dominant wavelength is unaffected. At a critical Deborah number, $De_{\mathrm{c}} = 1.677$, growth rate diverges at the most dominant wavenumber $K = K_{\mathrm{m}} = 1.97$, similar to the predictions of Wu and Chou [12]. Beyond De_{c}, the growth rate diverges for two wavenumbers (on each side of $K = 1.97$) between which now lies a region of stability. The maximum of the negative growth rate, in the stable window of wavenumbers (below $K = K_{\mathrm{c}}$), increases with increase

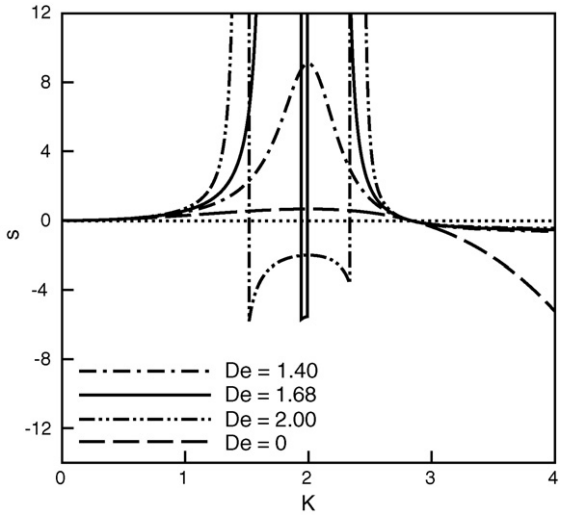

Fig. 2. Variation of growth rate with non-dimensional wavenumber K for different values of Deborah number De. For all cases, $H_0 = 0.5$, $\bar{\sigma} = 1000$, $\varepsilon = 2$, $\delta = 0$ and $R = 0$.

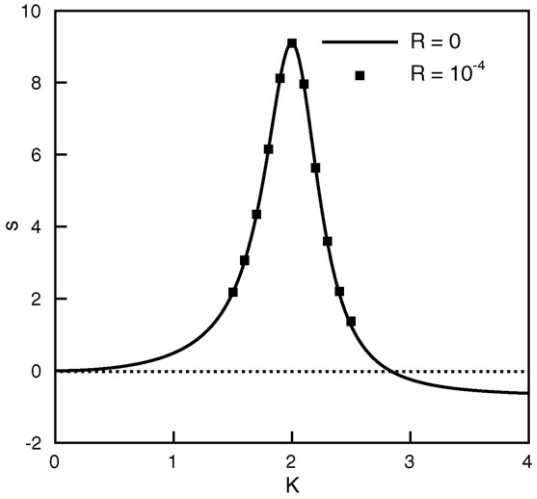

Fig. 3. Variation of growth rate with non-dimensional wavenumber K for cases with (a) $R = 0$, $\delta = 0$ and (b) $R = 10^{-4}$, $\delta = 0$. For all cases, $H_0 = 0.5$, $\bar{\sigma} = 1000$, $\varepsilon = 2$ and $De = 1.4$.

in De and asymptotically approaches zero. This maximum corresponds to the wavenumber $K = 1.97$, which is the dominant wavenumber for $De < De_c$. The window of stable wavenumbers widens with increase in De (Fig. 2). The left corner of the window asymptotically approaches $K = 0$ while the right corner approaches $K = K_c$, which is the critical wavenumber beyond which no wavenumber with a positive growth rate exists. The growth rate converges asymptotically to $s = -1/De$ for large wavenumbers ($K > K_c$).

The critical De, for which growth rate diverges at $K = K_m$, decreases with increase in H_0. For example, $H_0 = 0.3$, $De_c = 111.8$, while for $H_0 = 0.7$ is $De_c = 0.046$. In contrast to perfectly dielectric materials, in the case of leaky dielectrics, there is negligible potential drop in the liquid film and potential drop takes place mainly in the air gap. With increase in H_0, the air gap reduces and thus the normal potential gradient increases. This leads to large electric field strengths resulting in large magnitude of force on the free surface. Therefore, even a small elastic component yields a divergence with increase in H_0. Wu and Chou [12] suggested that the occurrence of the aforementioned unbounded growth rates explains the remarkably regular patterns observed in some experiments. They argued that for lower De, the growth rate changes smoothly with wavenumber and thus pillars (in the LISA process) of different sizes are possible. However, in cases when growth rate diverges, patterns would occur with a precise wavelength.

Interestingly, neglect of inertia seems to suggest that the dominant length scale of the instability depends not just on the energetic factors, but also on the Deborah number or the film rheology. As shown below, this non-physical conclusion stems from the neglect of inertia which should, by definition, become important for the ultrafast motion displayed at the divergence of the growth rate.

In the following sections, we explore the effect of inclusion of inertial terms and a small amount of solvent viscosity in the analysis.

4.2. *Effect of inertia on a thin film of a Maxwell liquid ($R \neq 0$, $\delta = 0$ and $De \neq 0$)*

We now examine the effect of inclusion of the inertial terms in the momentum equations on the non-physical singularity in growth rate observed for higher Deborah number in the case of polymer melts ($\delta = 0$) when the analysis was performed in the creeping-flow limit. The inertial stresses were neglected in view of typically small values of R (estimated to be $O(10^{-4})$), which multiplies the inertial terms in the momentum equation. However, in the cases when growth rate diverges, the product of a small R and a very large growth rate becomes $O(1)$ and must be included in the analysis.

Fig. 3 shows variation in the growth rate with wavenumber K for $R = 0$ and $R = 10^{-4}$ with $De = 1.4$ in both the cases. The results for the case with $R = 10^{-4}$ fall exactly on the curve with $R = 0$, thus showing for $De < De_c$, where growth rate is finite for all wavenumbers, the inertial term indeed has a negligible effect. This justifies the creeping-flow approximation whenever neglect of the inertia produces a well-behaved growth rate. However, for $De = 1.68$ the growth rate for $R = 0$ diverges, while the growth rate for $R = 10^{-4}$ is large but finite (Fig. 4). Note that for the most unstable root when $R = 10^{-4}$, there is no region of stable wavenumbers that exists below K_c for any value of De, in contrast to the case with $R = 0$. The "stable" zone that appears in the case of $R = 0$, however, is captured by the second root with $R \neq 0$, which always remains stable. Fig. 5 shows variation in the growth rate with K for $De = 2.0$. In contrast to the case with $R = 0$, no divergence was encountered for $R = 10^{-4}$. The maximum growth rate corresponds to the dominant wavenumber $K_m = 1.97$ which remains unchanged for all values of De irrespective of whether $De > De_c$ or $De < De_c$ in contrast to the case when inertial terms were neglected. We observe that for the wavenumbers where the growth rates are finite for $\delta = 0$, results for both $R = 0$ and $R = 10^{-4}$ agree well, and the two curves deviate only in a small window of wavenumbers where the $R = 0$ analysis predicts stable growth

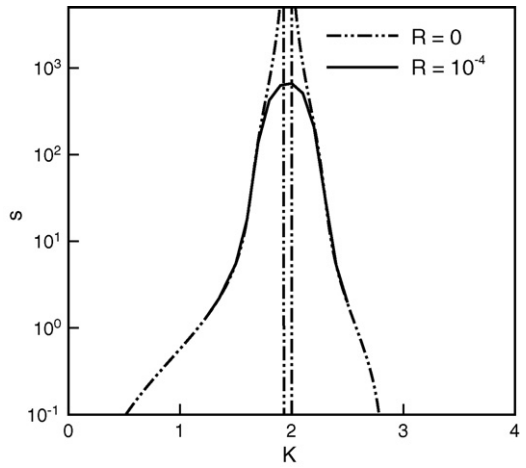

Fig. 4. Variation of growth rate with non-dimensional wavenumber K for cases with $R = 0$ and $R = 10^{-4}$. For all cases, $H_0 = 0.5$, $\bar{\sigma} = 1000$, $\varepsilon = 2$, $\delta = 0$ and $De = 1.68$.

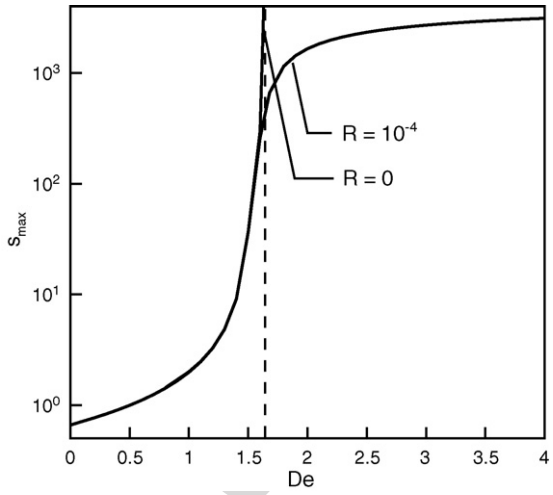

Fig. 6. Variation of maximum growth rate (at $K = 2.0$) with De for $R = 0$ and $R = 10^{-4}$. For all cases, $H_0 = 0.5$, $\bar{\sigma} = 1000$, $\varepsilon = 2$ and $\delta = 0$.

rates. For $R = 10^{-4}$, in that small window, growth rates are very high compared to the ones for neighboring wavenumbers. Thus, inclusion of inertia in the dynamics qualitatively alters the nature of the growth-rate vs wavenumber curve, yielding *only one* dominant lengthscale. The length scale of the patterns formed due to the instability therefore correspond to a very thin band of wavenumbers for which growth rates are very high and this provides a plausible explanation of the regularity of the lengthscale of patterns observed in some of the experiments [2].

Fig. 6 shows variation in the maximum growth rate with De. For $R = 0$, the growth rate diverges at $De = De_c$ (marked with a dashed line), whereas, for $R = 10^{-4}$, the growth rate is finite albeit being large. Below $De = De_c$, both the curves $R = 0$ and $R = 10^{-4}$ agree with each other, but beyond De_c they bifurcate with the maximum growth rate for $R = 0$ becoming infinite. The maximum growth rate asymptotically converges to a large finite value for large values of De for $R \neq 0$. Therefore,

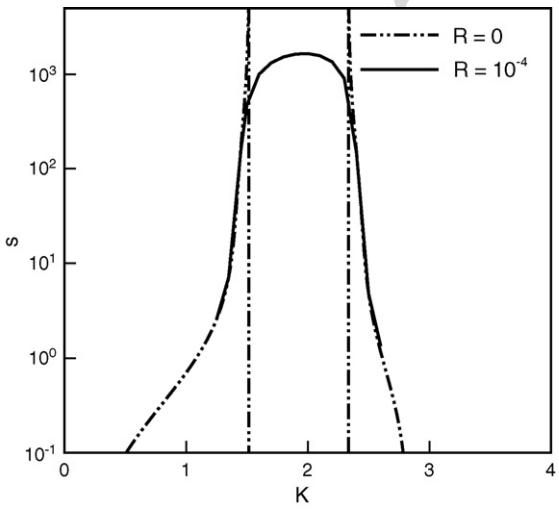

Fig. 5. Variation of growth rate with non-dimensional wavenumber K for cases with $R = 0$ and $R = 10^{-4}$. For all cases, $H_0 = 0.5$, $\bar{\sigma} = 1000$, $\varepsilon = 2$, $\delta = 0$ and $De = 2.0$.

while the creeping-flow approximation of neglecting inertial terms in the analysis is valid for $De < De_c$, when $De > De_c$, where the growth rate becomes unbounded for $R = 0$, inertial terms become important and must be retained in the analysis. A similar observation was made in the context of Rayleigh-Taylor instability of a viscoelastic liquid film by Aitken and Wilson [16].

For $De > De_c$, the relaxation time of the polymeric liquid is larger than the viscous flow time and the deformations in the viscoelastic liquid occur at time scales shorter than the relaxation time, implying that the polymeric liquid behaves more like an elastic solid. This elastic behavior of the polymeric liquid leads to instantaneous response in the absence of inertia, which manifests as a divergence in the growth rates. This seemingly instantaneous response of an elastic material in reality occurs in a finite, but very small time scale. With the inclusion of inertial terms, an incompressible purely elastic solid would permit shear waves with a very high traveling speed ($\sqrt{G/\rho}$), where G is the elastic modulus and ρ is the density of the material [19]. The time scale in a viscoelastic liquid for $De > De_c$ is dictated by a similar shear wave speed leading to very high but finite growth rates, thereby regularizing the singularity.

4.3. Behavior of a Jeffreys liquid in the absence of inertia ($R = 0$, $\delta \neq 0$, $De \neq 0$)

We next examine the case of a non-zero solvent viscosity in the limit $\delta \to 0$, but in the creeping-flow limit of $R = 0$. Fig. 7 shows variation of growth rate with wavenumber K for cases with $\delta = 0$ and $\delta = 10^{-3}$ (using the dispersion relation given in Appendix A). With increase in De from 1.0 to 1.4, the increase in elasticity of fluid enhances the instability, thus leading to increase in growth rate. At high De, even small amount of solvent viscosity dampens the growth rate and thus maximum growth rate is smaller for $\delta = 10^{-3}$ as compared to $\delta = 0$ for $De = 1.4$. This difference is negligible in the case with $De = 1.0$.

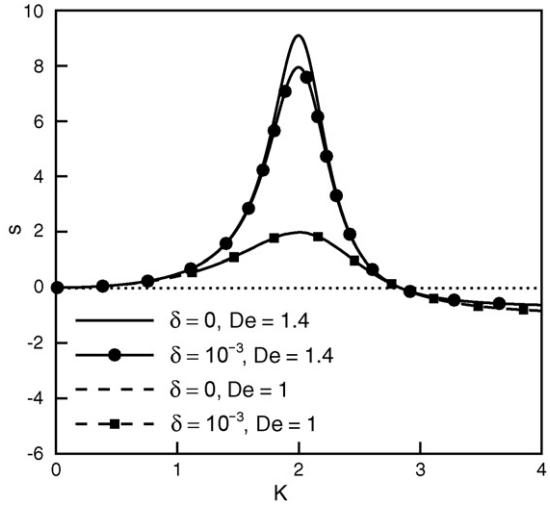

Fig. 7. Variation of growth rate with non-dimensional wavenumber K for cases with (a) $R = 0$, $\delta = 0$ and (b) $R = 0$, $\delta = 10^{-3}$. For all cases, $H_0 = 0.5$, $\bar{\sigma} = 1000$, $\varepsilon = 2$ and $De = 1.4$.

For $De > De_c$, the growth rate in cases with $\delta = 0$ diverges whereas with the inclusion of even a small amount of solvent viscosity ($\delta = 10^{-3}$) the singularity is smoothed out and finite positive growth rates are obtained for all De. In contrast to the case of $\delta = 0$, for $\delta \neq 0$ no region of stable wavenumbers is obtained below K_c, the critical wavenumber. Both the most dominant wavenumber as well as the critical wavenumber are found to be unaltered with increase in De for the case with $\delta = 10^{-3}$. Fig. 8 shows that for $De > De_c$, for which a divergence is observed for $\delta = 0$ and $R = 0$, a small amount of solvent viscosity removes the divergence and the growth rate becomes finite, albeit large. In contrast to the case $\delta = 0$, for $De = 2.0$, growth rate is finite in all regimes of wavenumber and no stable wavenumbers were encountered for wavenumbers less than the critical wavenumber (Fig. 9). In the region of wavenumbers, where growth rate is low, the curves for $\delta = 0$ and $\delta = 10^{-3}$

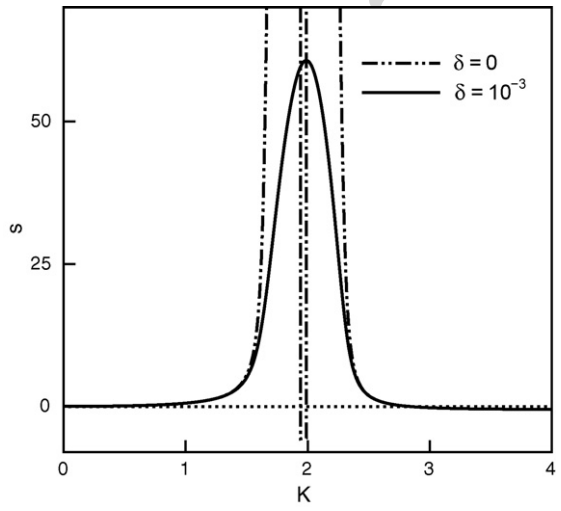

Fig. 8. Variation in growth rate with non-dimensional wavenumber K for cases with $\delta = 0$ and $\delta = 10^{-3}$. For all cases, $H_0 = 0.5$, $\bar{\sigma} = 1000$, $\varepsilon = 2$, $R = 0$ and $De = 1.68$.

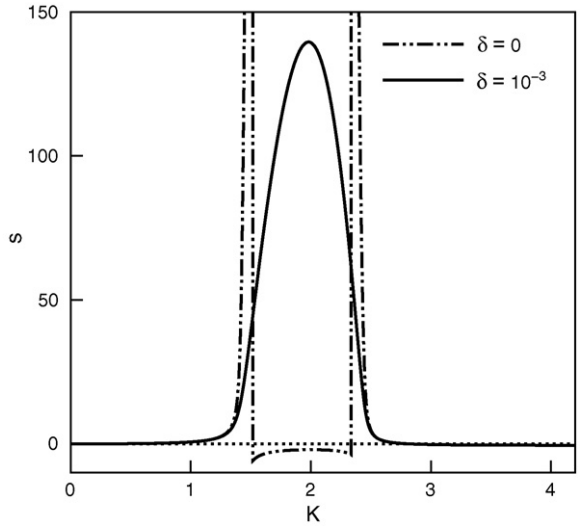

Fig. 9. Effect of a very small amount of solvent viscosity: variation in growth rate with non-dimensional wavenumber K for cases with $\delta = 0$ and $\delta = 10^{-3}$. For all cases, $H_0 = 0.5$, $\bar{\sigma} = 1000$, $\varepsilon = 2$, $R = 0$ and $De = 2.0$.

overlap. The growth rate in case with $De = 2.0$ is larger (twice) than that obtained for $De = 1.68$ due to the increased elastic component in the fluid.

Fig. 10 shows variation in maximum growth rate with De. The dashed line in the figure marks the De_c beyond which the growth rate diverges for the case $R = 0$ and $\delta = 0$. The curve for $\delta = 10^{-3}$ bifurcates from the one for $\delta = 0$ at large De (shows significant difference beyond $De \sim 1.4$). Beyond $De = De_c$, the growth rate for $\delta = 0$ is infinite, whereas it is finite for the case with $\delta = 10^{-3}$. The maximum growth rate asymptotically converges to a finite large value with increase in De for the case with $\delta \neq 0$. The physical reason behind the removal of singularity upon inclusion of solvent viscosity is that the added finite solvent viscosity provides an additional route for dissipation, the effect of which increases with increase in the growth rate and thus prevents the instability from growing in an unbounded manner.

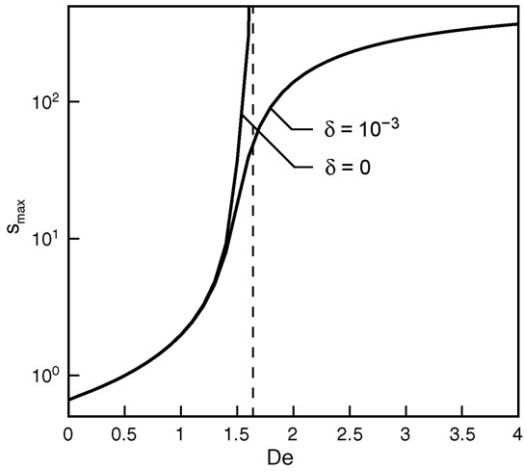

Fig. 10. Variation of maximum growth rate (at $K = 2.0$) with De for $\delta = 0$ and $\delta = 10^{-3}$. For all cases, $H_0 = 0.5$, $\bar{\sigma} = 1000$, $\varepsilon = 2$ and $R = 0$.

5. Conclusions

We have analyzed the surface instability of a confined viscoelastic liquid film due an applied electric field using the Maxwell and Jeffreys models for the liquid. The wavelength of this instability decreases while the growth rate increases with increase in the applied potential across the electrodes. The wavelength of the fastest growing mode (i.e. the dominant lengthscale of the instability) is found to be independent of the rheological properties such as relaxation time and solvent viscosity. This is a very important conclusion because in the absence of inertia, the dominant wavenumbers where the growth rate diverges *do* depend on the Deborah number or the film rheology. The independence of the instability on bulk rheology has also been found in an earlier study of a viscoelastic ultra-thin layer subjected to van der Waals interactions [15].

Beyond a critical value of melt elasticity ($De > De_c$), the instability growth rate diverges at two wavenumbers if fluid inertia is neglected. Further, in the inertia-less case, a window of stable wavenumbers is predicted between these two wavenumbers. Wu and Chou [12] also arrived at the same conclusion previously, based on a longwave analysis and attributed the highly regular patterns obtained in experiments to the infinite growth rate obtained for cases $De > De_c$. From a full dispersion relation valid for both short and long waves, we show that the non-physical behavior beyond the critical Deborah number cannot be attributed to the long wave approximation. In these cases, even the presence of a very small amount of inertia (as measured by the non-dimensional parameter R defined in this paper) removes the singularity in the growth rate and leads to a precisely defined dominant wavelength of the instability. The region of large growth rates around the dominant wavenumber is found to be narrow and the growth rate decreases sharply with small changes in the wavenumber in this region. The excellent fidelity and uniformity of polymer thin film microstructures created by electric field patterning is in agreement with a very sharp and prominent maximum of the growth rate over a very narrow window of wavenumbers.

Our study thus demonstrates that inclusion of inertia is essential in cases where due to an increase in the elastic contribution to the stress, viscoelastic fluids tend to behave more like elastic solids. In this regime, the response of the polymeric material is rather instantaneous in that it is dictated by a rapid, but finite, characteristic shear-wave speed. In such cases, the growth rate is large and its product with a small prefactor of inertial terms, R, cannot be neglected in the momentum equations.

We further showed that inclusion of a very small amount of solvent viscosity, as in the case of a polymer solution, also removes the singularity and leads to finite but large growth rates even in the absence of inertial effects. The physical reason for this behavior is that inclusion of solvent viscosity provides an additional route for energy dissipation in the system, thus slowing down the (otherwise infinite) growth rates in the molten polymer. The most dominant wavelength remains invariant with increase in De for any value of solvent viscosity and is predicted to be dependent only on the energetic parameters such as the destabilizing force and the surface tension, but not on rheological properties such as viscosity, relaxation time, retardation time, etc. We also showed that the growth rate for wavenumbers around the most dangerous wavenumber decreases very sharply. This suggests that the highly organized hexagonal features with precise length scales observed in experiments could be due to the large growth rate at a single wavenumber which arises as a consequence of the sharp decrease in the response time with increase in the elasticity of the fluid. Our study also has important implications in the derivation of non-linear evolution equations [7] describing the time-evolution of the morphology of the instability for polymer melts under the influence of electric fields; such derivations for Newtonian fluids usually invoke the creeping-flow approximation and neglect inertial stresses. For polymeric melts, our study points to the importance of including inertial effects in the derivation of the non-linear evolution equations. In conclusion, we have shown that the unbounded growth rates in viscoelastic liquids under the influence of an electric field is a consequence of the neglect of the inertial terms. Inclusion of inertial terms and/or solvent dynamics leads to finite, but large growth rates at a certain wavenumber which defines the dominant length scale and time scale of instability.

Appendix A

In this Appendix, we provide the elements of the characteristic matrix, whose determinant is set to zero to obtain the dispersion relation. It is useful to define a non-dimensional frequency-dependent viscosity $\bar{\eta}(s) \equiv \eta(s)/\eta_0$ which assumes values 1, $1/(1 + Des)$ or $(1 + De\delta s)/(1 + Des)$ for a Newtonian, Maxwell or Jeffreys liquid, respectively. The most general characteristic matrix (with the inclusion of inertia and solvent stresses) is denoted by a_{ij} whose non-zero components are:

$$a_{11} = -a_{13} = \sqrt{\frac{2}{\bar{\gamma}}} K H_0^{3/2}$$

$$a_{12} = a_{14} = a_{21} = a_{23} = a_{55} = a_{56} = 1$$

$$a_{31} = 2\sqrt{2}\bar{\eta} K H_0^{13/2} \mathrm{e}^{K(2+M)\sqrt{(2/\bar{\gamma})}H_0^{3/2}} \frac{(\sqrt{2}\bar{\gamma}^{3/2}K^3/\sqrt{H_0} + 8H_0 s\bar{\eta}(K^2 + s\bar{\eta}R))}{\bar{\gamma}^{5/2}}$$

$$a_{32} = 2\bar{\eta} H_0^5 \frac{(-\mathrm{e}^{K(2+M)H_0^{3/2}\sqrt{2/\bar{\gamma}}}(\sqrt{2/H_0}\bar{\gamma}^{3/2}K^3 + 8H_0 s(K^2 + s\bar{\eta}R)) + \mathrm{e}^{K(1+2M)H_0^{3/2}\sqrt{2/\bar{\gamma}}}(\sqrt{2/H_0}\bar{\gamma}^{3/2}K^3 + 4H_0 Ms\bar{\eta}(-K^2(M^2-3) + 2s\bar{\eta}R)))}{(\bar{\gamma}^2(M-1))}$$

$$a_{33} = 2\sqrt{2}\bar{\eta} K H_0^{13/2} \mathrm{e}^{K(2+M)\sqrt{(2/\bar{\gamma})}H_0^{3/2}} \frac{(\sqrt{2}\bar{\gamma}^{3/2}K^3/\sqrt{H_0} - 8H_0 s\bar{\eta}(K^2 + s\bar{\eta}R))}{\bar{\gamma}^{5/2}}$$

$$a_{34} = -2\bar{\eta} H_0^5 \frac{(\mathrm{e}^{KMH_0^{3/2}\sqrt{2/\bar{\gamma}}}(-\sqrt{2/H_0}\bar{\gamma}^{3/2}K^3 + 8H_0 s\bar{\eta}(K^2 + s\bar{\eta}R)) + \mathrm{e}^{KH_0^{3/2}\sqrt{2/\bar{\gamma}}}(\sqrt{2/H_0}\bar{\gamma}^{3/2}K^3 + 4H_0 Ms\bar{\eta}(K^2(M^2-3) - 2s\bar{\eta}R)))}{\bar{\gamma}^2(M-1)}$$

$$a_{37} = -\frac{8\sqrt{2}K^3 s\bar{\eta} H_0^{15/2} \mathrm{e}^{K(2+M)H_0^{3/2}(2/\bar{\gamma})^{1/2}}}{\bar{\gamma}^{5/2}}$$

$$a_{38} = \frac{8\sqrt{2}K^3 s\bar{\eta} H_0^{15/2} \mathrm{e}^{KMH_0^{3/2}(2/\bar{\gamma})^{1/2}}}{\bar{\gamma}^{5/2}}$$

$$a_{41} = \frac{4\bar{\eta}\mathrm{e}^{KH_0^{3/2}(2/\bar{\gamma})^{1/2}} H_0^3 K^2}{\bar{\gamma}}$$

$$a_{42} = \sqrt{2/\bar{\gamma}} H_0^{3/2} \bar{\eta} K \frac{(-2\mathrm{e}^{KH_0^{3/2}(2/\bar{\gamma})^{1/2}} + (1+M^2)\mathrm{e}^{KMH_0^{3/2}(2/\bar{\gamma})^{1/2}})}{(M-1)}$$

$$a_{43} = \frac{4\bar{\eta}\mathrm{e}^{-KH_0^{3/2}(2/\bar{\gamma})^{1/2}} H_0^3 K^2}{\bar{\gamma}}$$

$$a_{44} = -\sqrt{2/\bar{\gamma}} H_0^{3/2} \bar{\eta} K \frac{(-2\mathrm{e}^{-KH_0^{3/2}(2/\bar{\gamma})^{1/2}} + (1+M^2)\mathrm{e}^{-KMH_0^{3/2}(2/\bar{\gamma})^{1/2}})}{(M-1)}$$

$$a_{45} = -\frac{2\mathrm{e}^{KH_0^{3/2}(2/\bar{\gamma})^{1/2}} H_0^3 K^2}{\bar{\gamma}}$$

$$a_{46} = -\frac{2\mathrm{e}^{-KH_0^{3/2}(2/\bar{\gamma})^{1/2}} H_0^3 K^2}{\bar{\gamma}}$$

$$a_{67} = \mathrm{e}^{K(2H_0/\bar{\gamma})^{1/2}}$$

$$a_{68} = \mathrm{e}^{-K(2H_0/\bar{\gamma})^{1/2}}$$

$$a_{71} = -\frac{\bar{\gamma}\bar{\eta}\,\mathrm{e}^{KH_0^{3/2}(2/\bar{\gamma})^{1/2}}}{(2(H_0-1)^2 H_0 s\bar{\eta})}$$

$$a_{72} = \bar{\eta}\left(\frac{\bar{\gamma}}{H_0}\right)^{3/2} \frac{(\mathrm{e}^{KH_0^{3/2}(2/\bar{\gamma})^{1/2}} - \mathrm{e}^{KMH_0^{3/2}(2/\bar{\gamma})^{1/2}})}{(2\sqrt{2}K(M-1)(H_0-1)^2 H_0 s\bar{\eta})}$$

$$a_{73} = -\frac{\bar{\gamma}\bar{\eta}\,\mathrm{e}^{-KH_0^{3/2}(2/\bar{\gamma})^{1/2}}}{(2(H_0-1)^2 H_0 s\bar{\eta})}$$

$$a_{74} = -\bar{\eta}\left(\frac{\bar{\gamma}}{H_0}\right)^{3/2} \frac{(\mathrm{e}^{-KH_0^{3/2}(2/\bar{\gamma})^{1/2}} - \mathrm{e}^{-KMH_0^{3/2}(2/\bar{\gamma})^{1/2}})}{(2\sqrt{2}K(M-1)(H_0-1)^2 H_0 s\bar{\eta})}$$

$$a_{75} = \mathrm{e}^{KH_0^{3/2}(2/\bar{\gamma})^{1/2}} = \frac{1}{a_{76}} = -a_{77} = -\frac{1}{a_{78}}$$

$$a_{81} = 2\bar{\eta}\sqrt{\frac{2}{\bar{\gamma}}} H_0^{3/2} K\,\mathrm{e}^{KH_0^{3/2}(2/\bar{\gamma})^{1/2}}$$

$$a_{82} = -2\bar{\eta}\frac{(\mathrm{e}^{KH_0^{3/2}(2/\bar{\gamma})^{1/2}} - M\mathrm{e}^{KMH_0^{3/2}(2/\bar{\gamma})^{1/2}})}{(M-1)}$$

$$a_{83} = -2\bar{\eta}\sqrt{\frac{2}{\bar{\gamma}}} H_0^{3/2} K\mathrm{e}^{-KH_0^{3/2}(2/\bar{\gamma})^{1/2}}$$

$$a_{84} = -2\bar{\eta}\frac{(\mathrm{e}^{-KH_0^{3/2}(2/\bar{\gamma})^{1/2}} - M\mathrm{e}^{-KMH_0^{3/2}(2/\bar{\gamma})^{1/2}})}{(M-1)}$$

$$a_{85} = \frac{4\sqrt{2}H_0^{5/2}\mathrm{e}^{KH_0^{3/2}(2/\bar{\gamma})^{1/2}}(H_0-1)^2 K(\epsilon s\bar{\eta} + \bar{\sigma}\bar{\eta})}{(\bar{\gamma}^{3/2})}$$

$$a_{86} = -\frac{4\sqrt{2}\mathrm{e}^{-KH_0^{3/2}(2/\bar{\gamma})^{1/2}}(H_0-1)^2 H_0^{5/2} K(\epsilon s\bar{\eta} + \bar{\sigma}\bar{\eta})}{(\bar{\gamma}^{3/2})}$$

$$a_{87} = -\frac{4\sqrt{2}H_0^{5/2}e^{KH_0^{3/2}(2/\bar{\gamma})^{1/2}}(H_0-1)^2 Ks\bar{\eta}}{(\bar{\gamma}^{3/2})}$$

$$a_{88} = \frac{4\sqrt{2}H_0^{5/2}e^{-KH_0^{3/2}(2/\bar{\gamma})^{1/2}}(H_0-1)^2 Ks\bar{\eta}}{(\bar{\gamma}^{3/2})},$$

where $\bar{\eta} = (1 + De\delta s)/(1 + Des)$ and $M = \sqrt{1 + 2Rs/(\bar{\eta}K^2)}$.

References

[1] S.Y. Chou, L. Zhuang, Lithographically induced self-assembly of periodic polymer micro pillar arrays, J. Vac. Sci. Technol., B 17 (2000) 3197.

[2] S.Y. Chou, L. Zhuang, L. Guo, Lithographically induced self-construction of polymer microstructures for resistless patterning, Appl. Phys. Lett. 75 (1999) 1004.

[3] Z. Suo, J. Liang, Theory of lithographically-induced self-assembly, Appl. Phys. Lett. 78 (2001) 2971.

[4] L.F. Pease, W.B. Russel, Linear stability analysis of thin leaky dielectric films subjected to electric fields, J. Non-Newtonian Fluid Mech. 102 (2002) 233.

[5] E. Schaffer, T. Thurn-Albrecht, T.P. Russel, U. Stiener, Electrically induced structure formation and pattern transfer, Nature 403 (2000) 874.

[6] E. Schaffer, T. Thurn-Albrecht, T.P. Russel, U. Stiener, Electrohydrodynamic instability in polymer films, Europhys. Lett. 53 (2001) 518.

[7] V. Shankar, A. Sharma, Instability of the interface between thin fluid films subjected to electric fields, J. Colloid Interface Sci. 274 (2004) 294.

[8] R.V. Craster, O.K. Matar, Electrically induced pattern formation in thin leaky dielectric films, Phys. Fluids 17 (2005) 032104.

[9] R. Verma, A. Sharma, K. Kargupta, J. Bhaumik, Electric field induced instability and pattern formation in thin liquid films, Langmuir 21 (2005) 3710.

[10] N. Arun, A. Sharma, V. Shenoy, K.S. Narayan, Electric field controlled surface instabilities in soft elastic films, Adv. Mater. 18 (2006) 660.

[11] V.B. Shenoy, A. Sharma, Pattern formation in thin solid film with interactions, Phys. Rev. Lett. 86 (2001) 119.

[12] L. Wu, S.Y. Chou, Electrohydrodynamic instability of a thin film of viscoelastic polymer underneath a lithographically manufactured mask, J. Non-Newtonian Fluid Mech. 125 (2005) 91.

[13] R.G. Larson, Constitutive Equations for Polymer Melts and Solutions, Butterworth, Stoneham, MA, 1988.

[14] R.B. Bird, R.C. Armstrong, O. Hassager, Dynamics of polymeric liquids, Fluid Mechanics, vol. 1, New York, 1987.

[15] G. Tomar, V. Shankar, S.K. Shukla, A. Sharma, G. Biswas, Instability and dynamics of thin viscoelastic liquid films, Eur. Phys. J. E 20 (2006) 185.

[16] L.S. Aitken, S.D.R. Wilson, Rayleigh-Taylor instability in elastic liquids, J. Non-Newtonian Fluid Mech. 49 (1993) 13.

[17] G.I. Taylor, The stability of a horizontal fluid interface in a vertical electric field, J. Fluid Mech. 22 (1965) 1.

[18] D.A. Saville, Electrohydrodynamics: The Taylor-Melcher leaky dielectric model, Annu. Rev. Fluid Mech. 29 (1997) 27.

[19] L.D. Landau, E.M. Lifshitz, Theory of Elasticity, vol. VII, Butterworth, London, 1995.